JGR Oceans

RESEARCH ARTICLE
10.1029/2021JC018236

Key Points:

- High-resolution velocity and density data from the German Bight Region of Freshwater Influence are used to assess M2 tidal properties and intra-tidal variability
- M2 tidal motion is a hybrid of standing and progressive waves, with the standing wave contribution dominating
- Periodic counter-rotation of upper- and lower-layer current trajectories during the tidal cycle is related to water column stratification

Supporting Information:

Supporting Information may be found in the online version of this article.

Correspondence to:

R. Kopte,
robert.kopte@ifg.uni-kiel.de

Citation:

Kopte, R., Becker, M., Holtermann, P., & Winter, C. (2022). Tides, stratification, and counter rotation: The German Bight ROFI in comparison to other regions of freshwater influence. *Journal of Geophysical Research: Oceans*, *127*, e2021JC018236. https://doi.org/10.1029/2021JC018236

Received 11 NOV 2021
Accepted 19 MAY 2022

Tides, Stratification, and Counter Rotation: The German Bight ROFI in Comparison to Other Regions of Freshwater Influence

Robert Kopte[1], Marius Becker[1], Peter Holtermann[2], and Christian Winter[1]

[1]Institute of Geosciences, Christian-Albrechts-Universität zu Kiel, Kiel, Germany, [2]Leibniz Institute for Baltic Research Warnemünde (IOW), Rostock, Germany

Abstract The characteristics of tidal velocity profiles and their relation to stratification are investigated based on high-resolution field data collected at four locations in the German Bight Region of Freshwater Influence (ROFI) in the North Sea. The deployments each include two to three tidal cycles and were conducted during field campaigns in August 2016 and May 2018. The depth-averaged semidiurnal tidal motion is dominated by a standing wave directed toward the coast, but modified by a smaller, coast-parallel progressive wave contribution. The time series of the tidal velocity profiles consistently show tidal asymmetries with higher flood than ebb velocities near the surface and counter-clockwise rotation of the velocity trajectories at depth. Near the surface, phase-locked periodic changes in the sense of rotation within the tidal cycle are evident for three deployments, resulting in periodic counter-rotation of the upper and lower layer. During these episodes, stratification of the water column is observed. Counter-rotation is initiated after a sudden decoupling developing from the surface downward, with subsequent rapid development of stratification and velocity shear. The observed decoupling is most likely triggered by advection of the plume-induced lateral surface density gradient by weakly sheared ebb currents toward the study site. Due to the dominance of the standing wave in the German Bight ROFI, the observed intra-tidal variations of stratification are more similar to the Liverpool Bay and differ significantly from the Rhine ROFI, where the tidal dynamics are controlled by a progressive Kelvin wave.

Plain Language Summary The water velocities in the German Bight are strongly influenced by river freshwater input and semidiurnal tides. While the freshwater input from the rivers has a stratifying effect, tidal motion as well as wind and waves induce mixing. These forces compete in controlling the state of the water column in a complex manner. In theory, tidal motion should describe elliptical paths. However, in reality, these ellipses can be modified for example, by periodically occurring stratification. To assess the characteristics of the semidiurnal tidal velocity profile and its variability, four instruments to measure current velocity profiles were deployed in the German Bight during August 2016 and May 2018. Measurements were carried out for the duration of up to three tidal cycles, accompanied by parallel profiles of water temperature and salinity taken from the anchored ship nearby. Results show that periodic stratification related to the river freshwater plume is associated with periodically counter-rotating tidal currents during the tidal cycle. The measurement position relative to the location of the density front of the plume appears to be critical for the occurrence of counter-rotation. The observed dynamics are qualitatively compared to two other well-studied coastal ocean regions of freshwater influence.

1. Introduction

The German Bight (in the following "DB" for "Deutsche Bucht") is located in the Southeast of the North Sea (Figures 1a and 1b), and strongly affected by freshwater inflow. This Region of Freshwater Influence (ROFI, Chegini et al., 2020) is characterized by complex bathymetry with a corner-shape coastline and shallow water in general, containing several embayments, islands and subsea valleys as well as the intertidal areas of the Wadden Sea (Figure 1a). The region is significantly influenced by tidal wave propagation, communicating the signal of the North Atlantic autonomous tides.

In general, ROFI systems are particularly dynamic sectors of the coastal zone (Simpson et al., 1993), where the lateral buoyancy input by rivers has a larger impact on the density stratification of the water column than the vertical buoyancy flux at the surface due to heating or cooling (e.g., Palmer & Polton, 2011). The lateral freshwater

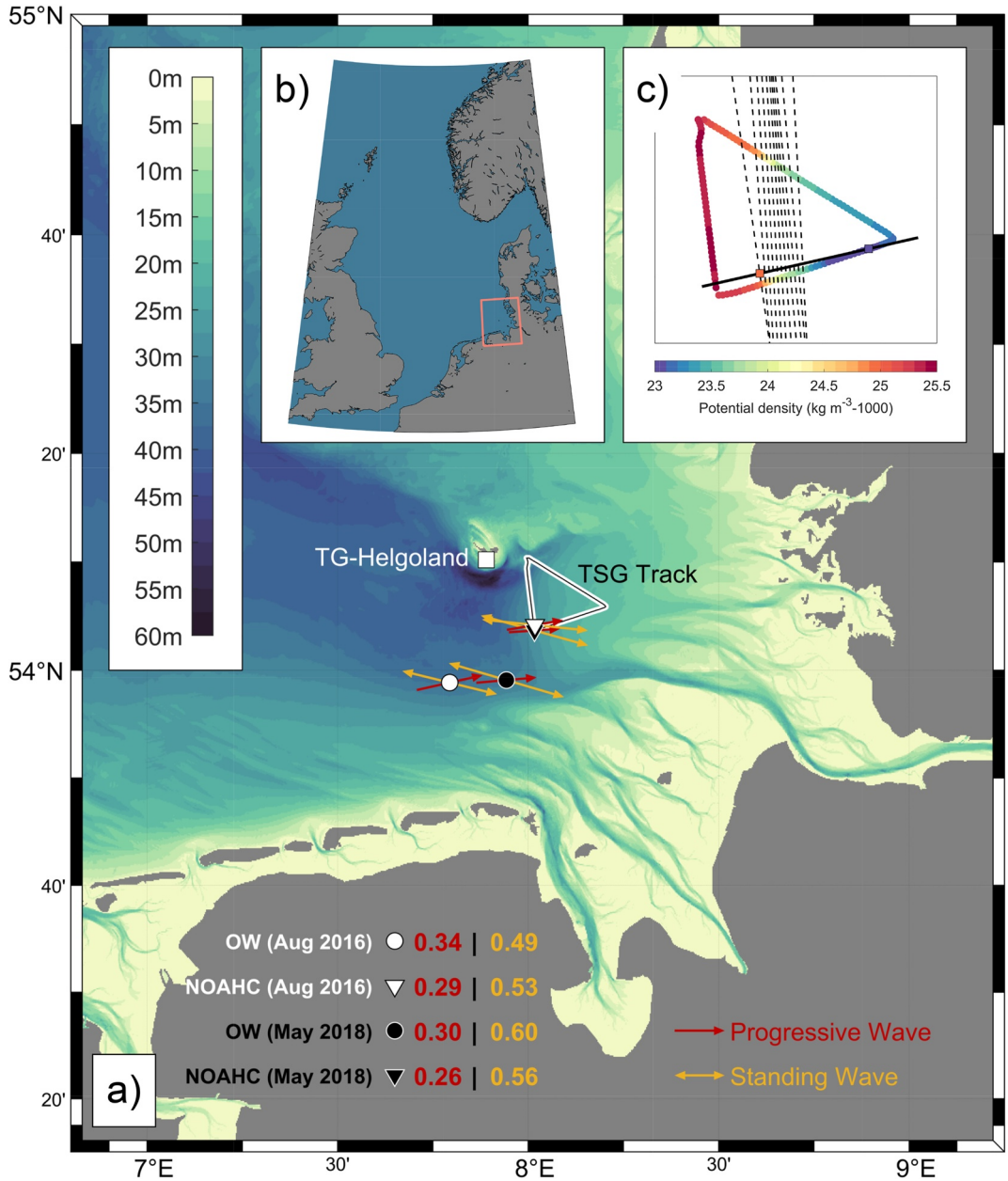

Figure 1. Study area. (a) German Bight with locations of measuring sites NOAHC (triangles) and OW (circles) during August 2016 (white) and May 2018 (black). Red and yellow arrows indicate progressive and standing wave contributions to the depth-averaged M2 tidal signal inferred from Acoustic Doppler Current Profiler (ADCP) current data at each measuring site (see Section 2.1.1). The amplitudes of the progressive and standing wave contributions (in m s^{-1}) at each location are displayed in corresponding colors in the lower part of the figure. The white square indicates the location of the Helgoland tide gauge, wind, and wave measurement station ("TG-Helgoland"). Also indicated is the track of thermosalinograph (TSG) measurements during R/V Heincke cruise HE510 in May 2018 as black line. (b) Overview map showing the location of the study area as part of the European North Sea. (c) Potential density distribution along the TSG track used for the estimation of the horizontal density gradient. Dashed black lines connect points of equal density on the southern and northern segments of the transect (approximating isopycnals). The thick black line displays the linear fit normal to these isopycnals and intersecting the point of minimum density along the track (see Section 2.2.2).

input drives an estuarine circulation, as lighter surface waters are transported seaward while denser waters flow landward in the lower layer. Stratification is determined by the competing effects of stratifying processes and mixing, caused by tides, wind, and waves. Alternating mixed and stratified conditions during one tidal cycle are considered to be controlled by strain-induced periodic stratification (SIPS, Simpson et al., 1990). The vertical

shear of the ebb and flood currents interacts with the horizontal density gradient maintained by the lateral freshwater input, periodically stratifying and homogenizing the water column. In turn, tidal ellipses respond to density straining, which is reflected in modifications of the vertical current structure. For a homogeneous water column with rectilinear surface currents, tidal ellipses tend to be weakly cyclonic at depth. By contrast, stratification may lead to the development of counter-rotating tidal ellipses, which result from the decoupling of surface and bottom waters due to a reduction in eddy viscosity at the pycnocline (e.g., Simpson & Souza, 1995). The upper layer then is less affected by bed friction. The anticyclonic rotary component of the flow is increased, while the concentration of frictional effects leads to an increase of the cyclonic rotary component in the lower layer. These dynamics are explained by the different effects of the pycnocline on cyclonically and anti-cyclonically rotating flows, which result in a different effective Ekman Layer thickness in each case. This is a consequence of the Earth's rotation and has been discussed in detail by Souza and Simpson (1996) and Visser et al. (1994).

For the semidiurnal tidal cycle, counter-rotating tidal currents associated with SIPS have been documented both at Liverpool Bay (Palmer, 2010; Verspecht et al., 2010) and the Rhine ROFI (de Boer et al., 2006; Fisher et al., 2002; Souza & Simpson, 1996; Visser et al., 1994). The two regimes differ in terms of the phasing of the occurrence of the counter-rotation and associated straining relative to the tidal motion. In the Rhine ROFI, maximum stratification (and therefore the occurrence of counter-rotation) is reached around high water, whereas at Liverpool Bay it is observed at low water. According to Fisher et al. (2002), these differences in the phasing are explained by the characteristics of the tidal wave. While in the Rhine ROFI the tidal motion is dominated by a progressive Kelvin wave, the tide in Liverpool Bay is a standing wave. Furthermore, the coast-parallel progressive wave interacts with a coast-normal density gradient, while in case of the standing wave, tidal motion and density gradient are directed parallel. Regardless of the timing of stratification, high-velocity shear associated with counter-rotation leads to periodically enhanced levels of the dissipation of turbulent kinetic energy (Fisher et al., 2002; Rippeth et al., 2001).

Similar evidence for SIPS-related modification of the tidal velocity profile have not been reported from observations for the DB ROFI to date, although the area is generally well-studied. Physical characteristics of the North Sea region are given by Sündermann and Pohlmann (2011) or Quante et al. (2016). Investigations of the circulation pattern in the DB area and its variability can be found in Port et al. (2011), Stanev et al. (2016), and Callies et al. (2017), based on observational data and/or numerical models. In a series of barotropic and baroclinic experiments using a 3D non-linear shelf model, Carbajal and Pohlmann (2004) investigated the influence of geometry and freshwater input on the M2 tidal ellipse properties, suggesting ellipse properties to undergo strong changes in response to irregular topography due to embayments and the deepening of the Elbe River. They also showed that the freshwater input in the DB induces anti-cyclonic rotation. General agreement was found between the model data and surface current data measured by high-frequency radar. The influence of topographic and frictional effects on the distortion and transformation of the tidal wave in the shallow waters of the DB area was also discussed by Stanev et al. (2014) based on model data. Gräwe et al. (2014) analyzed the seasonal variation of the tide in the DB and showed an 8%–30% increase of the tidal sea surface elevation amplitudes during summer. The increase was explained by the less efficient transport of vertical momentum through the thermocline toward the sea floor. Chegini et al. (2020) investigated the temporal and spatial variability of stratification pattern in the DB in a high-resolution baroclinic ocean model, concluding that stratification in the DB is strongly affected by the competition between tidal straining and mixing on a number of time scales. Furthermore, they stressed the importance of the location of the river plume for the state of stratification at a particular location.

We continue these efforts of understanding DB ROFI tidal dynamics and stratification on the basis of high-resolution measurements of the vertical structure of tidal current ellipses. Concurrent measurements of the density distribution shed light on the complex relation between stratification and current structure. The article finally presents a description of semidiurnal tidal dynamics and the intra-tidal variability in the DB and provides a qualitative comparison of the DB characteristics with Liverpool Bay and the Rhine ROFI.

2. Data and Methods

2.1. Velocity Observations by Acoustic Doppler Current Profilers (ADCPs)

High-resolution time series of current velocity profiles covering two to three tidal cycles were collected during four independent deployments of ADCPs in the DB (Figure 1a). Measurements were carried out in August 2016

at site NOAHC (54.07°N, 8.02°E) and site Outer Weser ("OW", 53.98°N, 7.79°E) during R/V Heincke cruise HE470 (see also Chegini et al., 2020, where site NOAHC is labeled P1) and were repeated in May 2018 during R/V Heincke cruise HE510. In 2018, OW (53.98°N, 7.94°E) was located further east compared to 2016, while NOAHC (54.06°N, 8.02°E) was placed in close proximity to the 2016 study site.

At all locations, velocity observations were obtained by upward-looking 600 kHz Teledyne RDI Workhorse ADCPs, which were mounted on frames 2 m above the seafloor. The ADCPs were configured to operate in mode 1, recording ensembles of four individual pings every 3.2 s with a vertical resolution of 0.25 m.

During post-processing, velocities were transformed from beam to earth coordinates, subsampled to 1 m vertical resolution and 10 min averages. To account for the intra-tidal changes in water level elevation, velocity observations were analyzed using sigma-coordinates and a mean depth vector for reference.

2.1.1. Progressive and Standing Wave Contributions

Neglecting reflected waves and the influence of friction, the theoretical solution for a wave propagating parallel to a straight coastline is a progressive Kelvin wave (Pugh & Vassie, 1976). In this case, currents would be rectilinear with maxima at high and low water (zero phase difference). The interaction with irregular topography may produce a standing wave, for which currents are strongest at mid tide (90° phase difference). A tidal wave can have both progressive and standing wave contributions, resulting in a phase difference between maximum currents and water level in the range of 0°–90°. To assess the characteristic of the barotropic M2 tidal wave in the DB, the depth-averaged velocity time series from the four study sites are analyzed following a method described by Pugh and Vassie (1976): M2 sine and cosine functions are fitted to both the east-west and the north-south velocity components to obtain amplitudes and phases relative to the local high water. From these parameters, the amplitude and direction of the propagating and standing wave contributions to the tidal wave signal are derived.

2.1.2. Decomposition of the Tidal Current Ellipse Into Its Rotary Components

To analyze the vertical structure of the M2 tidal currents, the velocity distribution is decomposed into its cyclonic (counter-clockwise in the Northern Hemisphere) and anti-cyclonic (clockwise) rotary components (Gonella, 1972; Maas & van Haren, 1987; Prandle, 1982; Soulsby, 1983). In a first step, harmonic functions of frequency ω_{M2} of the form $u = a_u \cos(\omega_{M2}t - \phi_u)$ and $v = a_v \cos(\omega_{M2}t - \phi_v)$ are fitted to the velocity time series at each depth level to form the complex tidal velocity $w = u + iv$. During one tidal period $T = 2\pi/\omega_{M2}$, w will trace out an elliptic stream figure and can be decomposed into two oppositely rotating circular components of fixed amplitude $W_\pm$ and phases $\phi_\pm$, which are used to derive the four ellipse parameters (Prandle, 1982):

1. Semi-major axis: $U_{\mathrm{SEMA}} = W_+ + W_-$
2. Eccentricity: $e = (W_+ - W_-)\,/\,(W_+ + W_-)$
3. Inclination: $\psi = (\phi_- + \phi_+)\,/2$
4. Phase angle: $\theta = (\phi_- - \phi_+)\,/2$

2.2. Shipboard Hydrographic Measurements

During both measurement campaigns, CTD profiles were collected in the vicinity of the study sites. Small measurement uncertainties (0.002 mS cm^{-1} for C, 0.002 K for T) were achieved by regular calibration of the sensors in the lab. During the measurements, the ship was anchored in a distance of less than 500 m to the moored ADCPs described in Section 2.1. The casts were taken continuously and as fast as possible, resulting in typical measurement intervals of around 3 min between individual profiles covering between one and two tidal cycles concurrent to each ADCP deployment (see Figure 2 for temporal coverage of CTD measurements).

During *R/V* Heincke cruise HE510, continuous measurements of subsurface temperature and salinity were collected along the track by the on-board thermosalinograph (TSG). The TSG data were recorded continuously at a sampling rate of 4 Hz using a Seabird SBE21 system with an intake located at 4 m depth in the front of the ship. One-minute averages were used for the analysis.

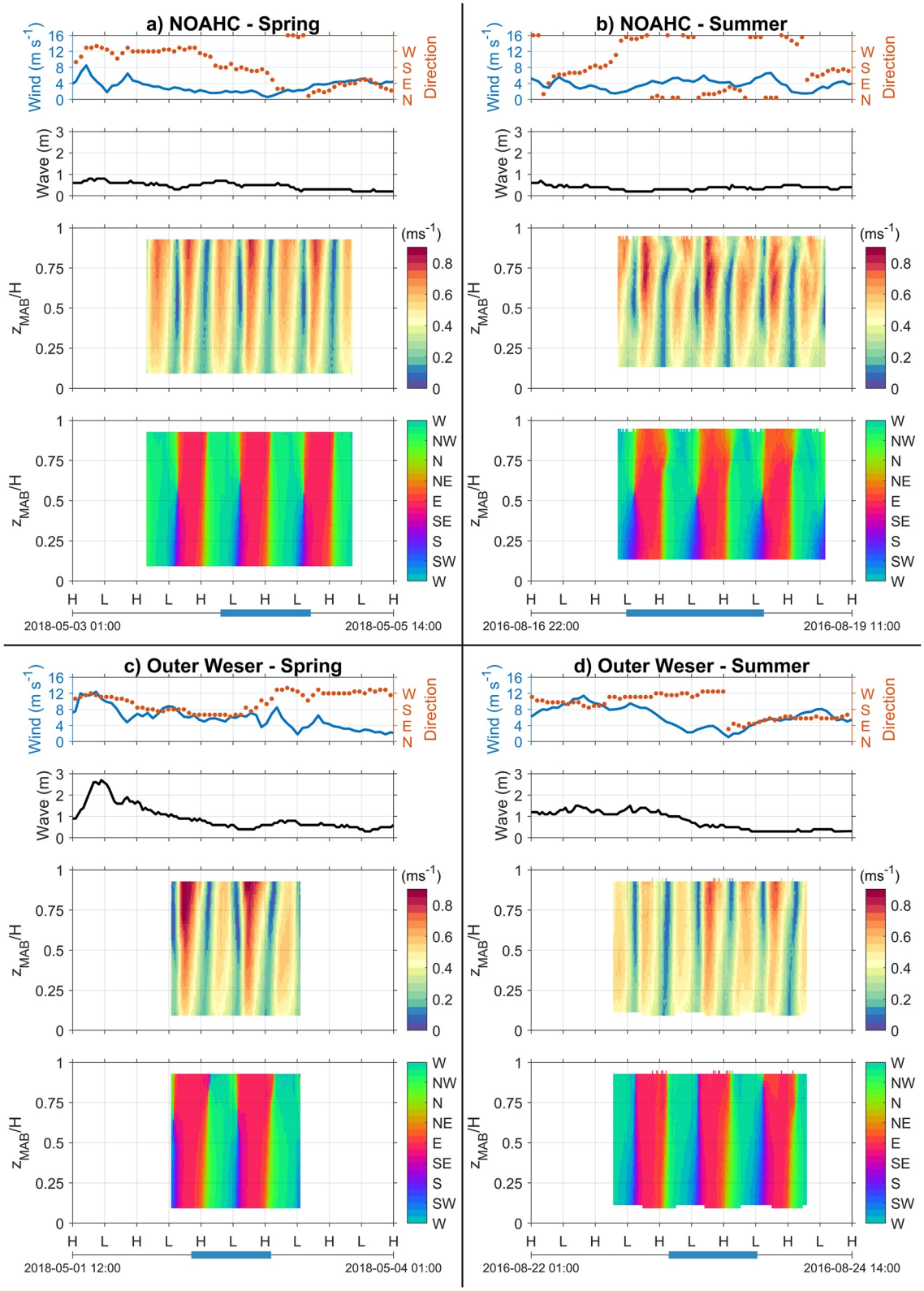
a) NOAHC - Spring
b) NOAHC - Summer
c) Outer Weser - Spring
d) Outer Weser - Summer
Wind (m s-1)
Direction
Wave (m)
zMAB/H
(ms-1)
W
NW
N
NE
E
SE
S
SW
H L H L H L H L H L H
2018-05-03 01:00
2018-05-05 14:00
2016-08-16 22:00
2016-08-19 11:00
2018-05-01 12:00
2018-05-04 01:00
2016-08-22 01:00
2016-08-24 14:00

Figure 2.

2.2.1. Stratification and Water Column Stability

The potential energy anomaly (PEA) reflects the condition of the water column in terms of stability and serves as a measure for stratification. It is defined as the change in potential energy relative to an unstratified, homogenous water column (Simpson & Bowers, 1981; Simpson et al., 1977):

$$\Phi = \frac{1}{D}\int_{-H}^{\eta} g z \left(\overline{\rho} - \rho\right) dz$$

with the depth-averaged density $\overline{\rho} = \frac{1}{D}\int_{-H}^{\eta} \rho dz$, the mean water depth H, the sea surface elevation η, the actual water depth $D = \eta + H$, and the gravitational acceleration g. Time series of PEA at each deployment site are derived from density profiles calculated from the CTD measurements (Section 2.2).

Another indicator for water column stability is the Gradient Richardson number (Richardson, 1920). It is determined as the ratio of the Brunt-Väisälä ($N^2 = -g\,\rho_0^{-1}\,\delta_z\rho$) and the vertical velocity shear ($S^2 = (\delta_z u)^2 + (\delta_z v)^2$):

$$Ri_g = \frac{N^2}{S^2}$$

Ri_g below the critical Richardson number $Ri_c = 0.25$ (e.g., M. Becker et al., 2018) indicate favorable conditions for turbulence production, either by a strong enough current shear to overcome stabilizing buoyancy forces ($0 \leq Ri_g \leq Ri_c$) or by static instability ($Ri_g < 0$).

2.2.2. Estimation of the Horizontal Density Gradient

To understand the dynamics caused by the interaction between tidal velocity and stratification, it is essential to know both the magnitude and the orientation of the local horizontal density gradient. Underway measurements of *R/V* Heincke's TSG (Section 2.2) are used for an estimation of the in situ conditions during the deployment of NOAHC in spring 2018. From the subsurface temperature and salinity data, the sea water density is calculated along the ship track in form of a triangle just to the northeast of the location of NOAHC (Figures 1a and 1c). The displayed track was covered within 1.5 hr around slack water to minimize falsifications of the gradient by advection of the density front by tidal currents. On the northern and southern segments, substantial along-track density gradients are observed, while the western segment shows relatively homogeneous surface water. Lines of equal density are derived for those parts of the northern and southern segments with strong gradients (isopycnals, dashed black lines in Figure 1c). A least squares fit of a straight line normal to the individual isopycnals and intersecting the point of minimum density along the track is used to derive both the magnitude and the orientation of the near-surface horizontal density gradient.

2.3. Tide Gauge, Wave Height, and Wind Data

Environmental data from a monitoring station near Helgoland (Figure 1) aided the interpretation of the tidal velocity observations. These included sea level data from the "HelgolandTG" tide gauge station (http://www.marineinsitu.eu/dashboard/) to integrate the hydrodynamic measurements into the fortnightly tidal spring-neap cycle. Measurements of wind speed and direction (DWD Climate Data Center [CDC], 2021) as well as sea state data (significant spectral wave height, https://seastate.bsh.de/rave/index.jsf) were analyzed to check for extraordinary/additional sources of mixing. Data from the Helgoland monitoring station was compared to concurrent time series from the monitoring station "Alte Weser." As records showed close agreement, but were more complete for the "Helgoland" station, only these data were chosen for display.

Figure 2. Observed tidal dynamics in the DB. Hovmoeller plots show the distribution of current speed (m s^{-1}, third row in each panel) and direction (fourth row) as measured by upward looking ADCPs at four locations in the German Bight (see Figure 1). Additionally, time series of wind speed and wind direction, as well as wave height (as recorded at the Helgoland tide gauge station) are shown to describe the environmental conditions before and during the deployments. *x*-axis marks times of High (H) and Low (L) Water. The observation period is indicated for each deployment at the bottom with blue bars marking the period of concurrent CTD coverage. A colorblindness-friendly version of this figure is included in Figure S1.

3. Results

3.1. Time Series of Tidal Current Dynamics

Due to the measurement locations particularly with regard to the local sources of freshwater and the different measurement periods, the four records of tidal dynamics (Figure 2) cover some of the range of boundary conditions and stratification states expected in the DB.

Considering the seasonal cycle, a more homogeneous water column is expected for the May 2018 measurements compared to August 2016, as the water column is potentially still partly mixed after the winter storms and thermal stratification is not yet fully established.

Further differences arise from the timing of the measurements with respect to the fortnightly tidal spring-neap cycle. Stratification can be substantially different between spring and neap tide conditions (Chegini et al., 2020). However, water level data from the Helgoland tide gauge station show that all measurements were made within a few days of spring tide, so the influence of the fortnightly cycle on the comparability of our results is considered negligible.

In general, the impact of wind and waves as mixing agents on meteorological time scales on the results presented here is considered small. Prevailing winds were predominantly south-westerlies with speeds of 3 to 5 m s^{-1} averaged over five tidal cycles before and during the measurement period (Figure 2). Nonetheless, slightly increased wind speeds of 8 to 10 m s^{-1} as well as a sudden change from westerly to easterly winds were observed shortly before and during the deployment of Outer Weser-Summer (Figure 2d). This needs to be kept in mind when interpreting hydrodynamic data from this deployment. Significant wave heights were on average smaller than 1 m, with the exception of a short period of wave heights of up to 3 m before the Outer Weser deployment in spring 2018.

As the local lateral input of buoyancy by river sources is most important in a ROFI system, the deployment position relative to the freshwater source plays an important role. In the DB, the main sources of freshwater are the rivers Elbe, Weser, and Ems (having average discharges of 861, 383, and 125 m^3 s^{-1}, respectively), with the Elbe and Weser discharging into the DB at the south-eastern boundary. Entering the DB, the freshwater plume is usually deflected to the right, that is, it will spread northward across the shallow parts of the northern Wadden Sea (Simpson, 1997). The NOAHC sites were located downstream at the northern flank of the Elbe valley (Figure 1a) and are therefore most likely affected by the Elbe river plume. The Outer Weser deployment of August 2016 was located offshore of the (probably weaker) Weser river plume, but not influenced by the Elbe river plume. This site therefore might experience a weaker stratification on average compared to the others. During the spring 2018 deployment, the Outer Weser site was located between the Weser and Elbe river plumes, potentially affected by both sources to some degree.

Thus, the main factors to keep in mind when interpreting potential differences between the study sites are their locations in the DB and their respective measurement periods with regard to the seasonal characteristics. The effect of wind (with the exception of the summer deployment of Outer Weser) and wave mixing as well as the timing of the observations with regard to the tidal spring-neap cycle is expected to be small.

Tidal velocity profiles (Figure 2) consistently show tidal asymmetries with maximum flood currents of 1.1 m s^{-1} and maximum ebb currents of 0.7 m s^{-1} near the surface. Velocities decrease with depth, accompanied by a slight phase advance of the near-bottom currents, however, the most pronounced baroclinic signature is observed at NOAHC-Summer (Figure 2b). Daily inequalities are most pronounced at Outer Weser-Summer (Figure 2d).

Compared to the absolute current speed, the pattern of the current direction is more complex (Figure 2). The lower half of the water column is generally characterized by counter-clockwise (cyclonic) rotation, as indicated by the gradual transition from westward (eastward) flow via southward (northward) flow to eastward (westward) flow. Except for the summer deployment of Outer Weser (Figure 2d), intra-tidal alterations of the ellipse rotation sense are evident in the upper half of the water column (Figures 2a–2c). While the ebb cycle is characterized by counter-clockwise rotation in the upper layer (same as in the lower layer), the flood period shows clockwise (anti-cyclonic) rotation in the upper layer. Illustrated by the node at mid-depth just after low water, this implies a counter-rotation of upper and lower layers observed at the three sites during flood. During the summer deployment of Outer Weser (Figure 2d) a depth-independent sense of rotation is observed for most of the measurement

period with a more gradual transition between eastward and westward flows at depth, that is, a more circular shape of the ellipse, while at the surface the change between ebb and flood currents occurs more rapidly, indicating a rather rectilinear flow.

3.2. Characterization of the M2 Tidal Signal

The tidal signal in the DB is dominated by semidiurnal constituents (Sündermann & Pohlmann, 2011). The characteristics of the barotropic M2 tidal wave at the study sites are assessed by the resolution of the depth-averaged velocity signal into progressive and standing wave contributions (see Section 2.1.1). At all four locations, the standing wave signal dominates with a mean amplitude of 0.55 m s^{-1} (standard error: 0.023 m s^{-1}), and is consistently directed toward the shallow areas in the south-eastern corner of the DB (Figure 1a). The progressive wave contribution is weaker (0.30 $\pm$ 0.016 m s^{-1}) and directed parallel to the large-scale (smoothed) coastline, representing the tidal Kelvin wave propagating cyclonically along the margins of the North Sea basin. Within the DB, the M2 tidal wave is therefore described as a superposition of progressive and standing waves. Consistent with a dominance of the standing wave signal but some influence of the progressive wave contribution, the peak tidal flows are reached shortly after mid-tide.

To describe the vertical structure of the semidiurnal tidal ellipses, the velocity distribution measured by the ADCPs are decomposed into their clockwise and counter-clockwise rotary components at M2 frequency (see Section 2.1.2). The derived M2 tidal ellipses (Figure 3) and the associated ellipse parameters (Figure 4) reveal a vertical structure that is in general agreement with theory. Near the seabed, tidal currents are counter-clockwise and their elliptical shape is most distinct. The amplitude of the semi-major axis increases with height above the sea floor (Figure 4a), accompanied by decreasing eccentricity (Figure 4b), which results in rectilinear currents in the subsurface layer at slightly different depths for the four deployments (Figure 3). Above the depth of rectilinear flow, tidal currents become more clockwise. At Outer Weser-Summer, the transition from counter-clockwise to rectilinear flow occurs just below the surface. In general, the spring deployments of NOAHC and Outer Weser show a very similar structure of tidal velocities. The most complex vertical structure is observed during the summer deployment of NOAHC that also differs notably from the structure observed at the site of Outer Weser-Summer, deployed only a few days later. In terms of the major axis orientation relative to the east-west direction (Figure 4c), a difference of approximately 6° between the spring and summer deployments is observed. In agreement with theory, near-bottom tidal ellipses lead near-surface ellipses. In general, lead times range between 20 and 30 min except for NOAHC-Summer, where the phase advance of near-bottom ellipses amounts to almost 1 hr (Figure 4d).

3.3. Intra-Tidal Variability Associated With Changes in Stratification

The description of the M2 tidal signal in the previous section does not take into account the variability within the tidal cycle. Nonetheless, substantial intra-tidal variability is observed in the velocity time series (Figure 2) and is investigated further in terms of its relation to stratification. Tidal currents and stratification are linked by tidal straining, which is the interaction of velocity shear with the local horizontal density gradient. The density distribution in the DB area is known to be highly variable on synoptic to interannual time scales (G. A. Becker et al., 1999; Chegini et al., 2020). It is constantly altered by the competing effects of freshwater input one the one hand, and tidal, wind and wave stirring on the other. Consequently, the measurement location relative to the position of the river plume plays a major role. Using a time series of TSG measurements during the spring campaign 2018, the strength and orientation of the horizontal density gradient in the vicinity of NOAHC is estimated (Section 2.2.2 and Figure 1c). The gradient is directed along the east-west axis, weakly tilted toward north-east at an angle of 8° and has a magnitude of ~2.7 kg m^{-4}. It reflects the transition between the freshwater of the Elbe-Weser plume and the saline water of the North Sea. This frontal region observed to the north-east of NOAHC (Figure 1c) presumably also exists directly to the east of the measuring site, where the northern flank of the Elbe River valley ends.

The summer deployment of NOAHC is characterized by persistent but highly variable stratification, which is expressed in high PEA values (Figure 5a). PEA values at Outer Weser-Summer remain low throughout the deployment period with only little variation. During the NOAHC and Outer Weser spring measurements, PEA values remain below the threshold for sustained stratification of 10 J m^{-3} (as defined in Chegini et al., 2020).

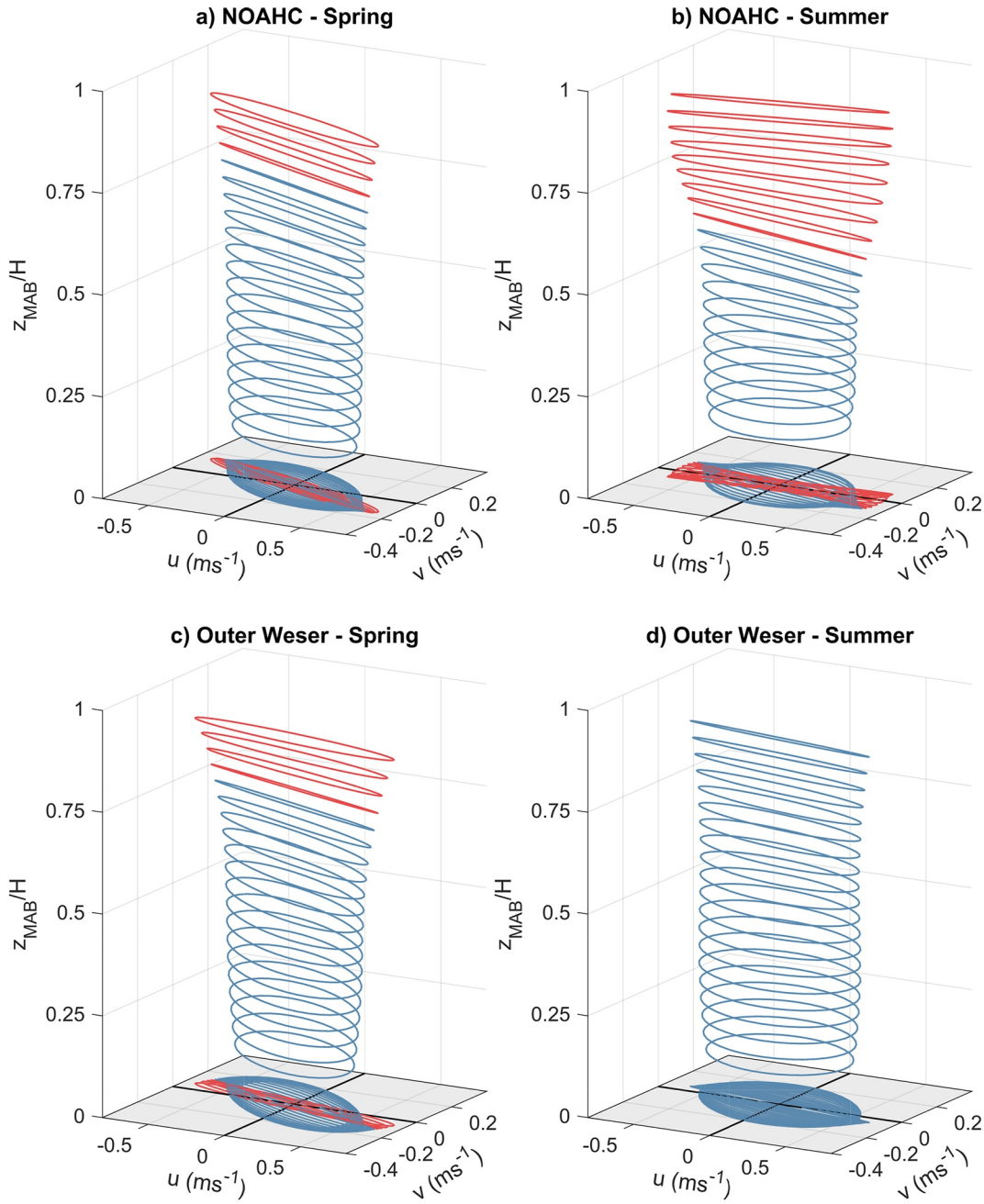

Figure 3. Vertical structure of M2 tidal current ellipses inferred from Acoustic Doppler Current Profiler (ADCP) current measurements. Red lines indicate anti-cyclonic (clockwise) rotation, while blue lines indicate cyclonic (counter-clockwise) rotation. Axis *u* refers to velocity in east-west direction, while *v* refers to velocity in north-south direction. At the bottom, individual current ellipses are stacked for an impression of the relative inclination between ellipses.

While the Outer Weser-Spring measurements indicate a secondary PEA maximum around high water, NOAHC-Spring expresses the clearest SIPS characteristic with a maximum stratification shortly after low water and low PEA values throughout the rest of the tidal cycle.

The bottom minor, surface major, and bottom major components of the tidal flow (Figures 5c–5e) show very similar trends during the tidal cycle for all four sites, largely reflecting the M2 signal and generally showing only weak intra-tidal variability. In contrast, strong variability and substantial differences between the sites are observed in the surface minor flow component (Figure 5b). Concurrently to the increase in PEA just before low

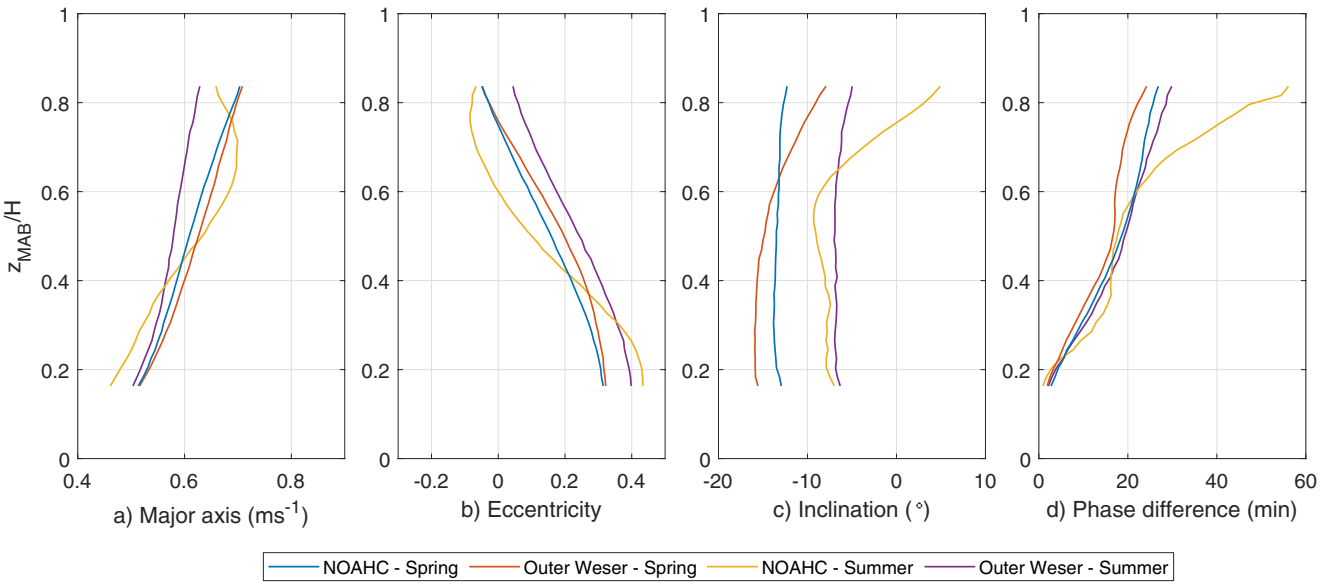

Figure 4. Ellipse properties at M2 tidal frequency as function of normalized depth: (a) major axis amplitude, (b) eccentricity, (c) major axis inclination relative to the east-west direction, (d) relative vertical phase difference. The upper and lower 15% of the water column are disregarded.

water (Figure 5a), a sudden shift toward positive surface minor velocities is observed at NOAHC-Spring, Outer Weser-Spring and to some extent also at NOAHC-Summer. In combination with the negative bottom minor flow (Figure 5c), this results in the development of vertical velocity shear in the minor direction of the flow and the existence of periodic counter-rotation of the tidal ellipses as long as surface minor and bottom minor velocities have different signs. At NOAHC-Spring the simultaneous occurrence of counter-rotation and stratification (compare Figures 5a and 5b) is indicative for influence of tidal straining. At Outer Weser-Summer, surface minor velocities are generally weakest, implying a rather rectilinear flow back and forth along the major tidal axis. Together with the cyclonic ellipse rotation at depth, the corresponding vertical structure of the flow reflects the theoretical solution resulting from the different scales of boundary layers for cyclonic and anticyclonic motions (Souza & Simpson, 1996; Visser et al., 1994).

Where periodic stratification is observed, the tidal trajectories in the upper layer do not entirely correspond to elliptical stream figures (Figures 6a–6c), which is not reflected by the analysis of the M2 signal (Section 3.2 and Figure 3). As a consequence of the intra-tidal variability in the minor flow component (Figure 5b), the tidal trajectory of the upper layer goes back and forth along only one half of the elliptical orbit. In the spring deployment of NOAHC (Figure 6a), a sudden change of direction in the upper layer trajectory is observed shortly after the maximum ebb current. It is precisely at this time, when the tidal trajectories of the upper and lower layers drift apart, that a simultaneous and sudden increase in PEA is observed. PEA values remain elevated during the transition from ebb to flood currents, and reduce as maximum flood currents are reached, which is accompanied by a reduction of the vertical velocity shear.

At NOAHC-Summer, where stratification persists throughout the tidal cycle and vertical velocity shear is generally higher compared to the other measuring sites, PEA levels are smallest around slack water, while maximum PEA values are reached during maximum ebb and flood (Figure 6b).

The comparatively weakest stratification occurs at Outer Weser-Summer, which shows symmetric tidal current trajectories in both upper and lower layers, accompanied by rather small PEA values (Figure 6d).

4. Discussion

This article presents high-resolution tidal current profiles from four short period ADCP deployments in the German Bight ROFI (Figure 1a), each accompanied by parallel shipboard CTD profiles at the measuring sites. The observations are used to describe the characteristics of the semidiurnal M2 tide and to investigate the intra-tidal variability of the vertical current structure in relation to the state of stratification.

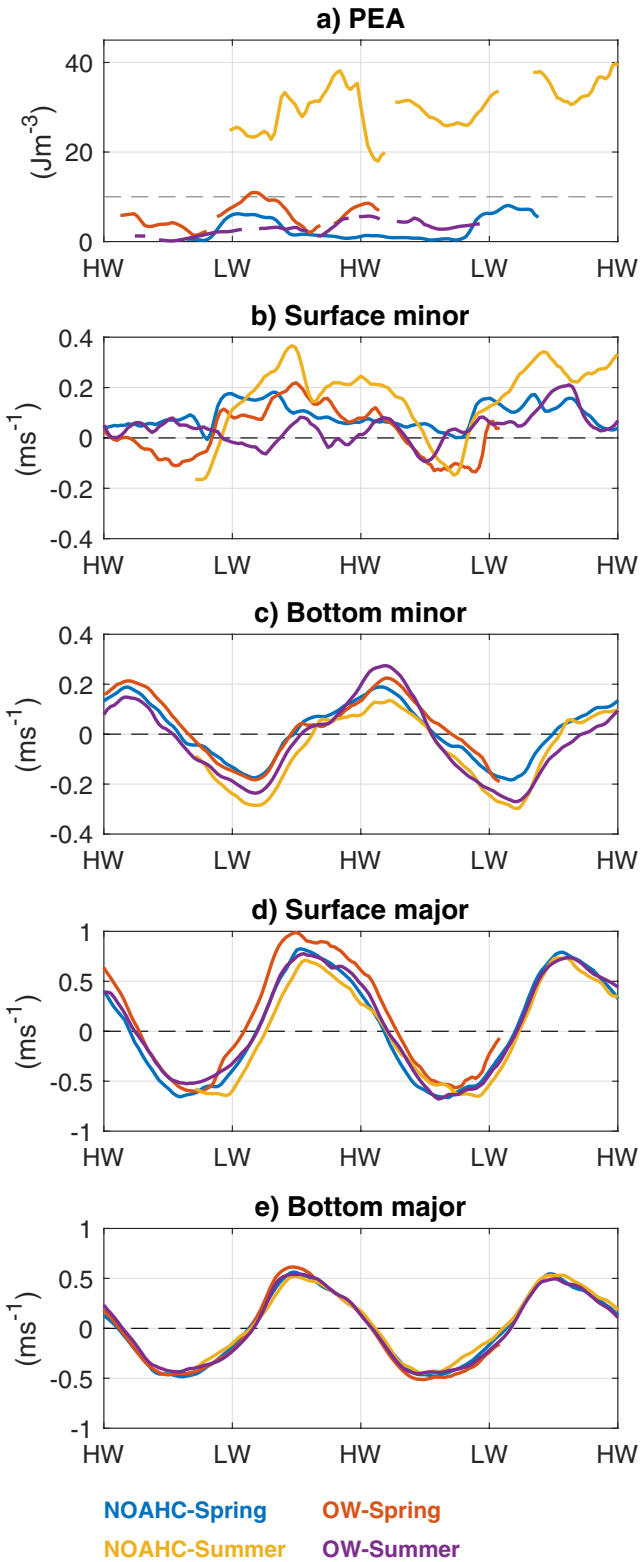

Figure 5. Time series of (a) potential energy anomaly (PEA, J m^{-3}), (b) minor axis surface flow (m s^{-1}), (c) minor axis bottom flow (m s^{-1}), (d) major axis surface flow (m s^{-1}), and (e) major axis bottom flow (m s^{-1}) color-coded for deployments as indicated. Time series are referenced to local high water. Dashed gray line in (a) indicates the PEA level above which the water column is considered stably stratified (10 J m^{-3}, Chegini et al., 2020).

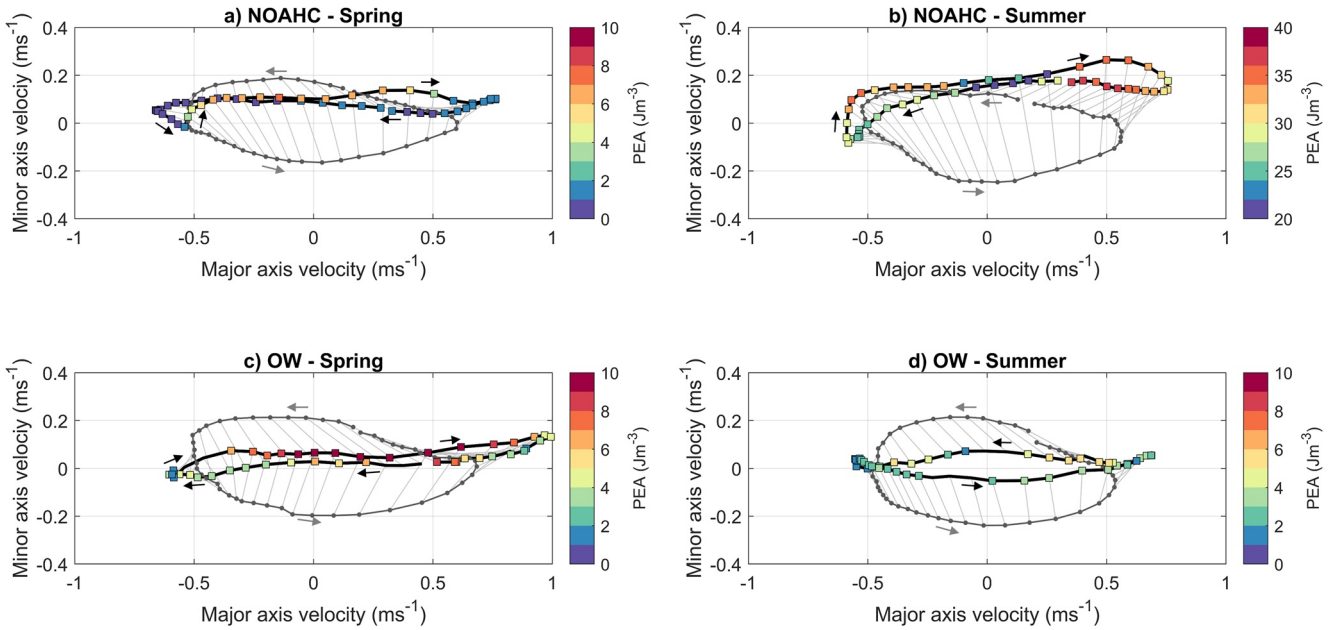

Figure 6. Trajectories of tidal currents depth-averaged for the upper layer (top-most 8 m, black lines) and lower layer (lowest 8 m, gray lines) at each deployment as indicated. Colored squares show the potential energy anomaly (PEA, J m^{-3}, note different color scales). Black and gray arrows indicate the direction of upper and lower tidal trajectories, respectively. Light-gray lines show the direction and strength of velocity shear between upper and lower layers at each point of the tidal cycle. Note that individual tidal cycles have been averaged with reference to the tidal phase to derive average ellipse trajectories.

4.1. German Bight M2 Tide Characteristics

On a larger scale, the semidiurnal tidal wave in the North Sea is described by a cyclonic, amphidromic system with a progressive Kelvin wave propagating along the coastline (Sündermann & Pohlmann, 2011). Near the coast, due to interactions with topography and the increasing influence of bed friction, also standing wave contributions can be produced (e.g., Pugh & Vassie, 1976). The location of the DB ROFI in the southeastern corner of the North Sea combined with complex topography and subsea valleys promotes the dominance of the standing wave contribution over the progressive wave signal observed in the depth-averaged M2 tidal velocity at all four sampling sites (Figure 1a). According to Sündermann and Pohlmann (2011), the progressive Kelvin wave is strongly dissipated by bottom friction in shallow water along the southeastern coast. Therefore, the M2 tide in the DB ROFI is a hybrid of both wave contributions, and differs substantially from the Rhine ROFI and the Liverpool Bay, which are prototypes for ROFIs dominated by either a purely progressive wave or a standing wave (e.g., Fisher et al., 2002, Figure 7).

A gradual vertical transition from counter-clockwise to clockwise rotation of the semidiurnal tidal ellipse is observed for the three DB measuring sites where (periodic) stratification is observed during the deployment periods (Figures 3 and 5a). Although observed upper layer current trajectories do not describe clear elliptical paths but are more complex (Figures 6a–6c), the derived M2 tidal ellipses could be interpreted as an indicator for the net sense of rotation of the tidal currents within one tidal cycle at a given depth level. The fact that variability away from the M2 frequency is neglected should generally be considered when interpreting fitted tidal ellipses from more complex environments.

4.2. Differences in Intra-Tidal Variability During Summer

During the summer deployment of NOAHC, persistent stratification of varying strength was measured. The corresponding tidal currents show a more complex structure compared to the other deployments, presumably caused by the strong and permanent decoupling of the upper from the lower layer. This is mirrored in maximum lead times of bottom currents over surface currents by up to 1 hr (Figure 4d) and pronounced veering of the tidal ellipses at different depths (Figure 4c). By contrast, the summer deployment of Outer Weser is characterized by a rather well-mixed water column (Figure 5a), considerably small variations in the vertical structure of the

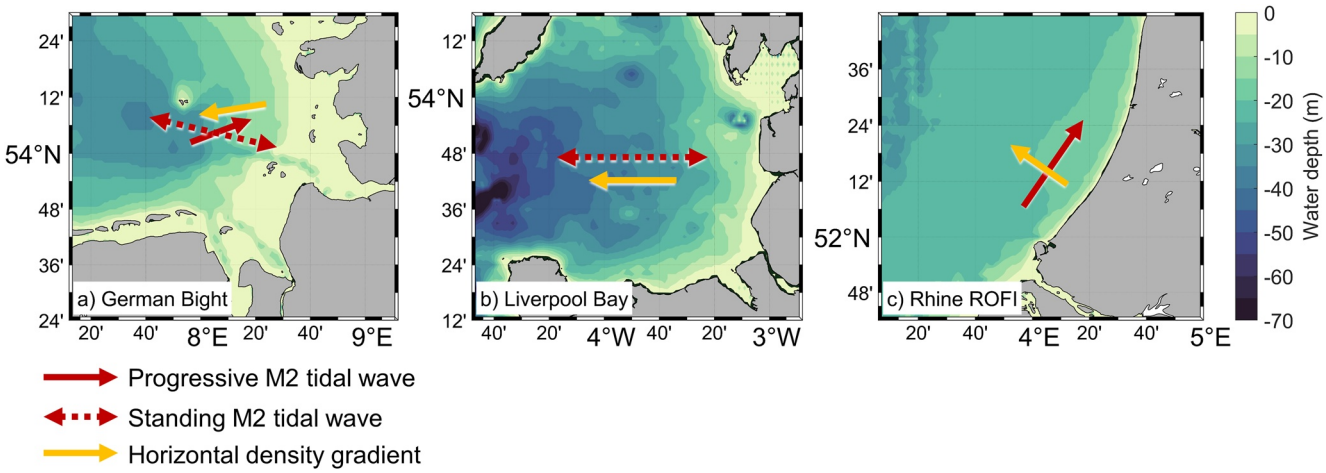

Figure 7. Schematic comparison of (a) German Bight, (b) Liverpool Bay, and (c) Rhine Region of Freshwater Influence (ROFI) regarding their M2 tidal wave characteristics and the relative orientation of wave propagation and horizontal density gradient.

ellipse properties (Figure 4) and no counter-rotation (Figure 3d). Remarkably, the measurements at the two sites took place only a few days apart, but at rather different positions relative to the (presumed) location of the river plume, suggesting that the measurement location relative to any freshwater source is more important for the state of stratification and consequently for the tidal dynamics than any other seasonal effect (solar heating, seasonal variability in river run-off, etc.) even on comparatively small spatial scales within one ROFI system. This implies, that also the spatial variability of the river plume position should be considered, which varies on a broad range of temporal and spatial scales (Chegini et al., 2020). Additionally, synoptic-scale variability associated with winds should be taken into account, as a period of elevated wind speed was observed just before and during the first half of the summer deployment of Outer Weser (Figure 2d), which could have temporarily induced comparatively more mixing and homogenization of the water column. An impact of the winds on the Outer Weser-Summer measurements seems even more likely, as toward the end of the deployment period, close to the surface after low water, indications for the occurrence of counter-rotation are observed (Figure 2d), likely associated with periodic stratification.

4.3. DB SIPS-Dynamics Compared to Liverpool Bay and the Rhine ROFI

Most of the intra-tidal variability observed in the DB measurements is associated with the surface minor component of the tidal flow (Figure 5b). Although a clear link between the PEA and the tidal velocity trajectory is difficult to establish based on the available data, SIPS-like behavior is observed especially during the spring deployments of NOAHC (Figure 6a) and to some extent also Outer Weser (Figure 6c).

Semidiurnal SIPS dynamics have been observed in the Liverpool Bay ROFI (Palmer, 2010; Verspecht et al., 2010), where the tidal motion resembles a standing wave and the horizontal density gradient is directed parallel to the major tidal axis (Figure 7b). Differential advection during ebb tide stabilizes the water column by moving lighter surface water faster offshore than the more saline water below, while during flood the effect reverses. Consequently, in Liverpool Bay, maximum stratification is reached at low water.

SIPS-dynamics in the Rhine ROFI differ substantially from those observed in the Liverpool Bay (Boer et al., 2006; Fisher et al., 2002; Simpson & Souza, 1995; Visser et al., 1994), especially with respect to the phasing of the stratification cycle. The tide in the Rhine ROFI is dominated by a coast-parallel progressive Kelvin wave interacting with a horizontal density gradient in the offshore direction (normal to the wave propagation axis, Figure 7c). Simpson and Souza (1995) noted that the presence of a mean vertical stratification is a necessary condition for SIPS to work in the Rhine ROFI. In stratified conditions, the spreading river plume results in decoupling and counter-rotating tidal ellipses in the upper and the lower layer. Tidal straining is then caused by the interaction of the minor component of the tidal flow with the offshore density gradient. During flood, minor velocities are directed

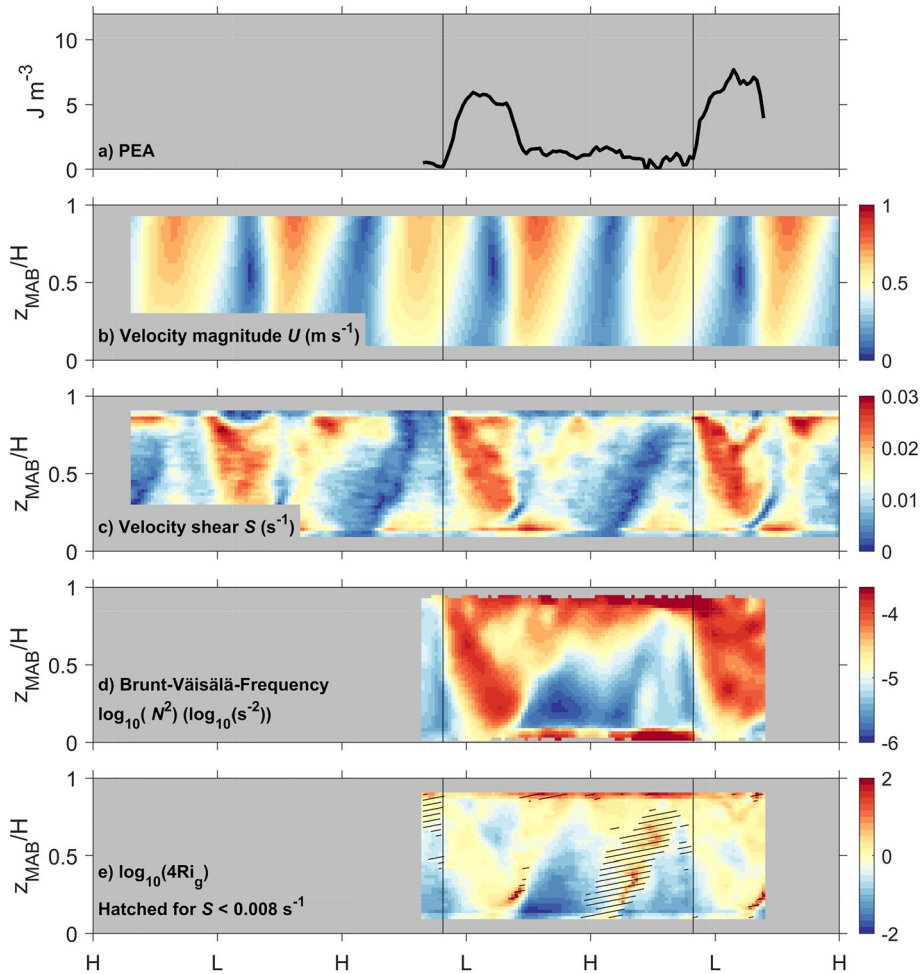

Figure 8. Water column stability around the inflection points displayed for the deployment of NOAHC-Spring. (a) Potential energy anomaly (PEA) showing sudden increases in stratification just before low water (L) indicated by black, vertical lines, (b) Velocity magnitude (m s^{-1}), (c) velocity shear (s^{-1}), (d) Brunt-Väisälä Frequency ($\log_{10}(s^{-2})$), (e) Gradient-Richardson number Ri_G, with red (blue) colors indicating the probability of reduced (increased) mixing, while yellow colors indicate critical conditions regarding the stability. In (e) areas are hatched, where the velocity shear is smaller than 0.008 s^{-1}.

offshore (onshore) in the upper (lower) layer, thereby further straining the density distribution. Consequently, maximum stratification is observed at high water, when maximum flood currents are reached. During ebb tide, onshore (offshore) minor velocities in the upper (lower) layer subsequently relax the water column.

Since in the DB ROFI tidal motions are dominated by the standing wave contribution, the observed dynamics bear similarities with Liverpool Bay rather than the Rhine ROFI. For the DB spring deployments, maximum stratification is observed shortly after low water, with the small phase shift probably explained by the influence of the progressive wave contribution. Also, (mean) stratification in both the DB ROFI (observed maximum vertical density difference <1.5 kg m^{-3}) and Liverpool Bay (2 kg m^{-3}, Verspecht et al., 2010) is rather weak, compared to a strong background stratification observed in the Rhine ROFI (3–8 kg m^{-3}, e.g., Visser et al., 1994). It should be noted, that the orientation of the horizontal density gradient in the DB (Figures 1c and 7a) allows in principle for interaction with both the major and minor components of the tidal flow, which might further complicate the picture.

Remarkably, at NOAHC, the vertical decoupling and associated onset of counter-rotation takes place rapidly just after low water, after the occurrence of maximum ebb currents. Thereafter, a positive feedback between stratification and differential advection temporarily enforces the decoupling of the water column and the development

of shear between upper and lower layer. As soon as the flood currents are sufficiently strong to homogenize the water column, which is indicated by decreasing PEA values toward the end of the flood cycle, the velocity shear continuously decreases and counter-rotation ceases (Figure 6a).

Rapid decoupling of the water column with the subsequent simultaneous development of strong vertical velocity shear and stratification was observed in Liverpool Bay by Verspecht et al. (2010). They referred to the moment of the decoupling as the "inflection point", which marks the time of maximum shear between the upper and lower layer along the main tidal axis.

At this moment, vertical motions are suppressed in the emerging pycnocline, allowing the geostrophic component to become important in the surface layer. According to Verspecht et al. (2010), the sudden decoupling is promoted by varying degrees of horizontal density gradients in the upper and lower layers, which also appears to be a necessary condition for the decoupling observed during the spring deployment of NOAHC in the DB (Figures 6a and 8). There, stratification starts to build up near the surface already before the inflection point is reached (Figure 8d). Expressed by the Gradient Richardson number (Section 2.2.1), the stability of the water column increases slightly before the inflection point, reaching critical values (Figure 8e). However, the vertical velocity shear remains small until the inflection point is reached (Figure 8c), and is therefore unlikely to account for the increase in water column stability (Figure 8e). This implies that classical SIPS dynamics, where stratification is the consequence of differential advection caused by velocity shear, are unlikely to trigger the inflection and therefore the decoupling of the upper and lower layer.

The proximity of the measurement location to the density front along the Elbe-Weser river plume (Figure 1) suggests that stratified water is initially advected toward the measurement site by the weakly sheared ebb currents (Figures 8b and 8c). As soon as a certain level of stratification is reached (i.e., directly at the inflection point), the water column decouples. With the resulting onset of counter-rotation in the upper layer, the associated velocity shear (Figure 8c) subsequently causes differential advection, thereby straining the density distribution and further stratifying the water column (Figure 8d) according to classical SIPS dynamics. The advection of the freshwater plume, and thereby the advection of a strong horizontal density gradient at the water surface, appears as a necessary condition to trigger the decoupling, which is then enhanced by SIPS. Based on a prognostic equation for PEA (Burchard & Hofmeister, 2008), Chegini et al. (2020) investigated processes of stratification and de-stratification in the DB area and found advection to strongly control local changes in stratification. They also stated that the state of stratification is affected by the position of the river plume. For the here suggested pre-conditioning of the water column by plume advection to trigger decoupling and counter-rotation, the measurement site is thus required to be located within the range of the tidal excursion of the strongest gradient. Given the geometry of the DB, it is therefore likely, that a critical region exists in form of a band of limited lateral extent along the main density front of the plume, where tidal dynamics resemble those observed at NOAHC. However, the actual nature of the proposed processes requires both longer observation periods and greater spatial coverage, especially to resolve the dynamics of the plume advection, which should be the aim of future studies.

Data Availability Statement

ADCP velocity data and CTD data from the 2016 deployments NOAHC-Summer and OW-Summer are available at https://doi.org/10.1594/PANGAEA.919168 and https://doi.pangaea.de/10.1594/PANGAEA.943958, respectively. ADCP and CTD data from 2018 deployments NOAHC-Spring and OW-Spring are available at https://doi.pangaea.de/10.1594/PANGAEA.943955. TSG data from *R/V* Heincke cruise 510 is available at https://doi.org/10.1594/PANGAEA.897214. Tide gauge sea level data (station "HelgolandTG") were downloaded and accessed on 25 April 2020 from http://www.marineinsitu.eu/dashboard. Hourly averages of wind speed and direction data from station 2115 (station "Helgoland") were downloaded and accessed on 6 April from https://opendata.dwd.de/climate_environment/CDC/observations_germany/climate/hourly/wind/historical/. Sea state data were accessed via the BSH Sea State Portal.

Acknowledgments
This study is supported by KMS-Kiel Marine Science, the Center for Interdisciplinary Marine Science at Kiel University. R. Kopte was funded by the Underway Research Data Project of the German Marine Research Alliance. Financing of P. Holtermann was provided by the German Research Foundation (DFG) through the grant HO 589/1-1. The authors gratefully acknowledge the help of Gabriel Herbst, Knut Krämer, and colleagues during data collection and thank the captain and crew of *R/V* Heincke for their support during the field campaigns HE470 and HE510. The authors thank the calibration lab of the Leibniz Institute for Baltic Research Warnemünde (IOW) for calibration of the CTD sensors. Tide gauge data were collected by the Waterways and Shipping Office Toenning and made freely available by the Copernicus project and the programs that contribute to it. Access to wind speed and direction data were provided by Deutscher Wetterdienst via the Climate Data Center. Sea state data were collected and made freely available by the BSH marine environmental monitoring network (MARNET), the RAVE project (www.rave-offshore.de), the FINO project (www.fino-offshore.de) and cooperation partners of the BSH. The sea state portal was realized by the RAVE project (Research at alpha ventus), which was funded by the Federal Ministry of Economics and Energy on the basis of a resolution of the German Bundestag. Open Access funding enabled and organized by Projekt DEAL.

References

Becker, G. A., Giese, H., Isert, K., König, P., Langenberg, H., Pohlmann, T., & Schrum, C. (1999). Mesoscale structures, fluxes, and water mass variability in the German Bight as exemplified in the KUSTOS- experiments and numerical models. *Deutsche Hydrographische Zeitschrift*, *51*(2–3), 155–179. https://doi.org/10.1007/BF02764173

Becker, M., Maushake, C., & Winter, C. (2018). Observations of mud-induced periodic stratification in a hyperturbid estuary. *Geophysical Research Letters*, *45*(11), 5461–5469. https://doi.org/10.1029/2018GL077966

Burchard, H., & Hofmeister, R. (2008). A dynamic equation for the potential energy anomaly for analyzing mixing and stratification in estuaries and coastal seas. *Estuarine, Coastal, and Shelf Science*, *77*(4), 679–687. https://doi.org/10.1016/j.ecss.2007.10.025

Callies, U., Gaslikova, L., Kapitza, H., & Scharfe, M. (2017). German Bight residual current variability on a daily basis. Principal components of multi-decadal barotropic simulations. *Geo-Marine Letters*, *37*(2), 151–162. https://doi.org/10.1007/s00367-016-0466-2

Carbajal, N., & Pohlmann, T. (2004). Comparison between measured and calculated tidal ellipses in the German Bight. *Ocean Dynamics*, *54*(5), 520–530. https://doi.org/10.1007/s10236-004-0096-5

Chegini, F., Holtermann, P., Kerimoglu, O., Becker, M., Kreus, M., Klingbeil, K., et al. (2020). Processes of stratification and destratification during an extreme river discharge event in the German Bight ROFI. *Journal of Geophysical Research: Oceans*, *125*(8), C01022. https://doi.org/10.1029/2019JC015987

de Boer, J., Pietrzak, J. D., & Winterwerp, J. C. (2006). On the vertical structure of the Rhine region of freshwater influence. *Ocean Dynamics*, *56*(3–4), 198–216. https://doi.org/10.1007/s10236-005-0042-1

DWD Climate Data Center (CDC). (2021). *Historical hourly station observations of wind speed and wind direction for Germany*. Version v21.3.

Fisher, N. R., Simpson, J. H., & Howarth, M. J. (2002). Turbulent dissipation in the Rhine ROFI forced by tidal flow and wind stress. *Journal of Sea Research*, *48*(4), 249–258. https://doi.org/10.1016/S1385-1101(02)00194-6

Gonella, J. (1972). A rotary-component method for analyzing meteorological and oceanographic vector time series. *Deep-Sea Research and Oceanographic Abstracts*, *19*(12), 833–846. https://doi.org/10.1016/0011-7471(72)90002-2

Gräwe, U., Burchard, H., Müller, M., & Schuttelaars, H. M. (2014). Seasonal variability in M2 and M4 tidal constituents and its implications for the coastal residual sediment transport. *Geophysical Research Letters*, *41*(15), 5563–5570. https://doi.org/10.1002/2014GL060517

Maas, L. R. M., & van Haren, J. J. M. (1987). Observations on the vertical structure of tidal and inertial currents in the central North Sea. *Journal of Marine Research*, *45*(2), 293–318. https://doi.org/10.1357/002224087788401106

Palmer, M. R. (2010). The modification of current ellipses by stratification in the Liverpool Bay ROFI. *Ocean Dynamics*, *60*(2), 219–226. https://doi.org/10.1007/s10236-009-0246-x

Palmer, M. R., & Polton, J. A. (2011). A strain-induced freshwater pump in the Liverpool Bay ROFI. *Ocean Dynamics*, *61*(11), 1905–1915. https://doi.org/10.1007/s10236-011-0430-7

Port, A., Gurgel, K.-W., Staneva, J., Schulz-Stellenfleth, J., & Stanev, E. V. (2011). Tidal and wind-driven surface currents in the German Bight. HFR observations versus model simulations. *Ocean Dynamics*, *61*(10), 1567–1585. https://doi.org/10.1007/s10236-011-0412-9

Prandle, D. (1982). The vertical structure of tidal currents. *Geophysical & Astrophysical Fluid Dynamics*, *22*(1–2), 29–49. https://doi.org/10.1080/03091928208221735

Pugh, D. T., & Vassie, J. M. (1976). Tide and surge propagation off-shore in the dowsing region of the North Sea. *Deutsche Hydrographische Zeitschrift*, *29*(5), 163–213. https://doi.org/10.1007/BF02226659

Quante, M., Colijn, F., Bakker, J. P., Härdtle, W., Heinrich, H., Lefebvre, C., et al. (2016). Introduction to the assessment—Characteristics of the region. In M. Quante & F. Colijn (Eds.), *North Sea region climate change assessment* (pp. 1–52). Springer International Publishing (Regional Climate Studies). https://doi.org/10.1007/978-3-319-39745-0_1

Richardson, L. F. (1920). The supply of energy from and to atmospheric eddies. *Proceedings of the Royal Society of London. Series A*, *97*(686), 354–373. https://doi.org/10.1098/rspa.1920.0039

Rippeth, T. P., Fisher, N. R., & Simpson, J. H. (2001). The cycle of turbulent dissipation in the presence of tidal straining. *Journal of Physical Oceanography*, *31*(8), 2458–2471. https://doi.org/10.1175/1520-0485(2001)031<2458:tcotdi>2.0.co;2

Simpson, J. H. (1997). Physical processes in the ROFI regime. *Journal of Marine Systems*, *12*(1–4), 3–15. https://doi.org/10.1016/S0924-7963(96)00085-1

Simpson, J. H., Bos, W. G., Schirmer, F., Souza, A. J., Rippeth, T. P., Jones, S. E., & Hydes, D. (1993). Periodic stratification in the Rhine ROFI in the North Sea. *Oceanologica Acta*, *16*(1), 23–32.

Simpson, J. H., & Bowers, D. (1981). Models of stratification and frontal movement in shelf seas. *Deep-Sea Research Part A. Oceanographic Research Papers*, *28*(7), 727–738. https://doi.org/10.1016/0198-0149(81)90132-1

Simpson, J. H., Brown, J., Matthews, J., & Allen, G. (1990). Tidal straining, density currents, and stirring in the control of estuarine stratification. *Estuaries*, *13*(2), 125. https://doi.org/10.2307/1351581

Simpson, J. H., Hughes, D. G., & Morris, N. C. G. (1977). The relation of seasonal stratification to tidal mixing on the continental shelf. In *A voyage of discovery. Deep-Sea Research (supplement)* (pp. 327–340). With assistance of M. Angel.

Simpson, J. H., & Souza, A. J. (1995). Semidiurnal switching of stratification in the region of freshwater influence of the Rhine. *Journal of Geophysical Research*, *100*(C4), 7037. https://doi.org/10.1029/95JC00067

Soulsby, R. L. (1983). The bottom boundary layer of shelf seas. In B. Johns (Ed.), *Elsevier Oceanography Series: Physical Oceanography of Coastal and Shelf Seas* (Vol. 35, pp. 189–266). Elsevier. https://doi.org/10.1016/s0422-9894(08)70503-8

Souza, A. J., & Simpson, J. H. (1996). Interaction between mean water column stability and tidal shear in the production of semidiurnal switching of stratification in the Rhine ROFI. In D. G. Aubrey & C. T. Friedrichs (Eds.), *Buoyancy effects on coastal and estuarine dynamics*. American Geophysical Union (AGU). https://doi.org/10.1029/ce053p0083

Stanev, E. V., Al-Nadhairi, R., Staneva, J., Schulz-Stellenfleth, J., Valle-Levinson, A., & Arnoldo (2014). Tidal wave transformations in the German Bight. *Ocean Dynamics*, *64*(7), 951–968. https://doi.org/10.1007/s10236-014-0733-6

Stanev, E. V., Schulz-Stellenfleth, J., Staneva, J., Grayek, S., Grashorn, S., Behrens, A., et al. (2016). Ocean forecasting for the German Bight. From regional to coastal scales. *Ocean Science*, *12*(5), 1105–1136. https://doi.org/10.5194/os-12-1105-2016

Sündermann, J., & Pohlmann, T. (2011). A brief analysis of North Sea physics. *Oceanologia*, *53*(3), 663–689. https://doi.org/10.5697/oc.53-3.663

Verspecht, F., Simpson, J. H., & Rippeth, T. P. (2010). Semidiurnal tidal ellipse variability in a region of freshwater influence. *Geophysical Research Letters*, *37*(18). https://doi.org/10.1029/2010GL044470

Visser, A., Souza, A., Hessner, K., & Simpson, J. (1994). The effect of stratification on tidal current profiles in a region of freshwater influence. *Oceanologica Acta*, *17*, 369–381.